Biomedical Signal Processing and Control 6 (2011) 395–404

Contents lists available at ScienceDirect

Biomedical Signal Processing and Control

journal homepage: www.elsevier.com/locate/bspc

Hair removal methods: A comparative study for dermoscopy images

Qaisar Abbas [a,b,*], M.E. Celebi [c], Irene Fondón García [d]

[a] Department of Computer Science and Technology, Huazhong University of Science and Technology, 1037 Luoyu Road, Wuhan 430074, China
[b] Center for Biomedical Imaging and Bioinformatics, Key Laboratory of Image Processing and Intelligent Control of Ministry of Education, Wuhan, China
[c] Department of Computer Science, Louisiana State University, Shreveport, LA, USA
[d] Department of Signal Theory and Communications, School of Engineering Path of Discovery, Sevilla, Spain

ARTICLE INFO

Article history:
Received 8 October 2010
Received in revised form 9 December 2010
Accepted 12 January 2011
Available online 5 February 2011

Keywords:
Skin cancer
Dermoscopy
Melanoma
Hair segmentation
Linear interpolation
Image inpainting
PDE
Fast marching

ABSTRACT

Removal and restoration of hair and hair-like regions within skin lesion images is needed so features within lesions can be more effectively analyzed for benign lesions, cancerous lesions, and for cancer discrimination. This paper refers to "melanoma texture" as a rationale for supporting the need for the proposed hair detection and repair techniques, which incompletely represents why hair removal is an important operation for skin lesion analysis. A comparative study of the state-of-the-art hair-repaired methods with a novel algorithm is also proposed by morphological and fast marching schemes. The hair-repaired techniques are evaluated in terms of computational, performance and tumor-disturb patterns (*TDP*) aspects. The comparisons have been done among (i) linear interpolation, inpainting by (ii) non-linear partial differential equation (*PDE*) and (iii) exemplar-based repairing techniques. The performance analysis of hair detection quality, was based on the evaluation of the hair detection error (*HDE*), quantified by statistical metrics and manually used to determine the hair lines from a dermatologist as the ground truth. The results are presented on a set of 100 dermoscopic images. For the two characteristics measured in the experiments the best method is the fast marching hair removal algorithm (*HDE*: 2.98%, *TDP*: 4.21%). This proposed algorithm repaired the texture of the melanoma, which becomes consistent with human vision. The comparisons results obtained, indicate that hair-repairing algorithm based on the fast marching method achieve an accurate result.

1. Introduction

Malignant melanoma (*MM*) [1] is increasing among white and non-white populations around the world. New Zealand Cancer Registry reported that the incident rate (2.3 per 100,000 to 4.3 per 100,000) of *MM* has been doubled over an 11-year period from 1996 to 2006. The curability of *MM* [2] is 100% if detected early. However, many expert dermatologists had estimated accuracy around 75–84% [3] for identification of melanomas.

Nearly all of the researchers in skin cancer diagnosis agree that melanomas can be automatically identified with the help of image processing and pattern recognition [4] techniques. In clinical studies of dermoscopy [5], *ABCD* (*A*: asymmetry, *B*: border, *C*: color, *D*: differential structures); pattern analysis; Menzies's method; and 7-point checklist rules are used for the classification of pigmented skin lesions (*PSL*) images. An automatic dermoscopic image classification system has typically four steps: (a) artifact and noise reduction, (b) boundary detection, (c) feature extraction and (d) pattern analysis as well as lesion classification.

Nowadays, border (*B*) detection and classification of pigmented skin lesions (*PSL*) stages are the most challenging tasks. To detect borders, there are many devoted methods trying to develop an unsupervised segmentation technique for dermoscopy. For instance, thresholding [6–8], region growing [9], clustering [10], Geodesic Active or Region-Based Contour models, *GAC* [11] and *RAC* [12] respectively, multi-direction Gradient Vector Flow (*GVF*) [13], *GVF* [14], and Dermatologist-like Tumor Extraction Algorithm (*DTEA*) [15] are common tumor segmentation methods. A different approach was developed in studies [16,17] to detect the lesion border by a radial search technique. In [18], a new Fuzzy C-means clustering algorithm was also developed. In order to improve tumor segmentation process, Gomez et al. [19] designed an unsupervised algorithm called the Independent Histogram Pursuit (*IHP*), for hyperspectral images of skin lesions. As occurs with the border detection stage, melanoma classification task is extremely difficult. In the literature, there are a few studies [20–23] devoted to the classification of *PSL* tumors. Since, the *MM* border detection and classification tasks are difficult for skin cancer analysis due to hair-like regions occluded the tumor.

* Corresponding author at: Computer Science and Technology, Center for Biomedical Imaging and Bioinformatics, Key Laboratory of Image Processing and Intelligent Control of Ministry of Education, Huazhong University of Science and Technology, 1037 Luoyu Road, Wuhan 430074, China. Tel.: +86 13437168375; fax: +86 27 87559091.

E-mail address: qaisarabbasphd@gmail.com (Q. Abbas).

1746-8094/$ – see front matter
doi:10.1016/j.bspc.2011.01.003

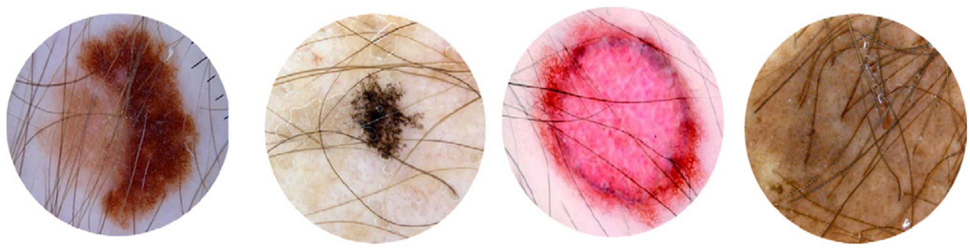

(a) (b) (c) (d)

Fig. 1. Difficulties to do melanoma classification in case of four skin tumors occluded with hair pixels for digital dermoscopy.

As shown in Fig. 1, hair pixels, usually present in dermoscopic images, occlude some of the information of the lesion such as its boundary and texture. Therefore, in melanoma recognition and classification tasks these hair artifacts must be removed. In a real-time *CAD* tool, an automatic hair removal method that preserves all the lesion features while keeping its computational cost low enough to be used is needed. However, hair problem has not been fully addressed in the literature. Ineffective hair removal algorithms lead toward over-segmentation [17] and poor pattern analysis, disturbing the tumor's patterns. In fact, to perform effective pattern analysis [24], an effective hair-repairing algorithm is required.

There are a few methods developed in the literature to repair thin and thick hair. These studies were mainly focused on measuring the hair detection error totally forgetting about the effect on tumor's patterns. As a result, these hair removal methods often leave behind undesirable blurring; disturb the texture of the tumor; and result in color bleeding. Moreover, these methods required high computational cost. They are mainly focused on designing a hair detection algorithm.

Hair-removal methods can be broadly classified as linear interpolation techniques, inpainting by non-linear-*PDE* based diffusion algorithms and exemplar-based methods. An example of linear interpolation hair removal algorithm can be found elsewhere [25–29]. In the literature on hair removal, a few papers, which utilized the concept of non-linear-*PDE* based diffusion, were presented, [11,30–32]. Also, little attention has been paid to remove hair by exemplar-based inpainting technique [12,33–35]. A detailed description and comparison of each hair removal method is presented in Section 2.

In this paper, a comparative study for several hair removal methods of the three classes: linear interpolation, inpainting by *PDE* non-linear diffusion and exemplar-based methods is presented. A fast and effective novel hair segmentation and repaired algorithm is also proposed. First, hairs are detected by a derivative of Gaussian (*DOG*) and subsequently enhanced by a morphological technique, which are inpainted by a modified fast marching method [36]. Also, the fast marching method is modified by changing color space from *RGB* to *CIE* $L^*a^*b^*$ uniform color space to adapt the results to human perception. Therefore, the proposed algorithm for hair-occluded information restoration is consistent with human vision without disturbing the melanoma texture.

The hair detection algorithms are applied to a set of 100 dermoscopic images and subsequently compared with the expected hair (ground truth) obtained by an experienced dermatologist. Hair detection and removal algorithms are evaluated in terms of computational cost and performance quality. To evaluate the hair detection error (*HDE*), a metric that takes into account different types of errors is computed, based on the ground truth. The performance analysis is carried out with the tumor-disturb patterns (*TDP*) analysis.

The remainder of this paper is organized as follows. In Section 2, information about three different types of hair-repairing algorithms is given. In Section 3, we introduce the key idea of our proposed hair detection and occluded information repairing method, explaining the use of a derivative of Gaussian (*DOG*), morphological and fast marching methods. Numerical results and comparisons based on simulations and statistical metrics on dermoscopic images are presented in Section 4. Finally, the paper concludes in Section 5.

2. Hair-occluded removal methods

As it has been already mentioned, if a skin lesion is covered by hair segmentation, pattern analysis and classification tasks will be affected by their high gradient. Therefore, an automatic method that preserves all the lesion features while keeping its computational cost low enough to be used in a real-time *CAD* tool is needed. In the following sections, the problems associated with the hair detection and removal algorithms by linear interpolation, non-linear *PDE*-based and exemplar-based inpainting methods are described in detail. In these subsections, we mainly focus on hair removal algorithms. Afterwards, novel feature-preserving hair detection and repairing algorithm is presented in Section 3.

2.1. Hair removal by linear interpolation methods

Lee et al. [25] proposed the DullRazor hair-removal algorithm that uses bilinear interpolation method to remove hair pixels. The algorithm consists of three basic steps: (1) identifying the dark hair locations by morphological closing operation; (2) replacing the hair pixels by bilinear interpolation; and (3) smoothing the final result by adaptive median filter. A similar interpolation method was used by Nguyen et al. [26]. The DullRazor algorithm includes an interpolation method to replace the non-hair pixels and smooth its results by median filter. However, this operation often leads to undesirable blurring and color bleeding. The morphological masks applied are limited to a number of discrete orientations and therefore it is sensitive to the orientation of the linear elements. Above of all these problems, the weakest point of the technique is it incapability to distinguish between hairs and line segments of the tumors patterns, disturbing the tumor's texture and therefore making the method unsuitable for dermoscopic images.

In [27], Schmid used a median filter to reduce the influence of small structures, such as hair, on the segmentation result. Similarly, the work of Saugeona et al. [28] and Fleming et al. [29] detect and remove hair using morphological operations and thresholding in *CIE* $L^*u^*v^*$ color space. In these techniques, a hair mask was generated by a fixed thresholding procedure on these thin structures based on their luminosity. At the end, each masked pixel was replaced by an average of its neighboring non-masked pixels via another morphological operation. Median and morphological filters often produce blur effect on tumor patterns. In practice, such interpolation methods do not consider the information provided by the neighboring regions that may affect tumor's texture and boundary. Hence, these linear interpolation methods are effective only when tumors are texture-less or do not contain hair pixels. In practice, dermoscopy images often do not satisfy these constraints.

2.2. Hair removal by non-linear PDE-based diffusion methods

A few articles on hair removal algorithms by non-linear-*PDE* diffusion based inpainting methods were also proposed in the past. The advantage of using non-linear diffusion over linear interpolation is that it utilizes neighboring information in a natural manner through non-linear diffusion, filling large gaps while maintaining a sharp boundary. A method based on non-linear *PDE*-diffusion was utilized in [11] and [30–32].

A number of algorithms specifically designed to work with non-linear-*PDE* inpainting method address the image filling issue. These image inpainting techniques fill the holes in the images by propagating linear structures (called isophotes in the inpainting literature) into the target region via diffusion. They are inspired by the *PDE* of physical heat flow, and work convincingly as restoration algorithms. As mentioned before, their main drawback is that the diffusion process introduces some blur, which becomes noticeable when filling hair regions.

In practice, the non-linear-*PDE* diffusion scheme is useful to track tumor boundary due to its edge-preserving capabilities. To the best of our knowledge, it can be used as a preprocessing step [11,30,31] before tumor detection. But, since diffusion affects the tumor's pattern, this scheme or morphological scheme by PDE [30] should not be used to remove hair from melanoma images. The *PDE*-diffusion method has a higher computational complexity than the linear interpolation method.

The general mathematical equation of non-linear diffusion for *PDE* proposed by Barcelos and Pires [31] is given as following:

$$\begin{aligned} &u_t = g\left|\nabla u\right| div(\nabla u/\left|\nabla u\right|) - \lambda(I-g)(u-I), \quad x \in \Omega, \quad t>0 \\ &u(x,0) = I(x), \quad x \in \Omega \subset R^2, \\ &\frac{\partial u}{\partial \eta}|_{\partial\Omega \times R} = 0, \quad x \in \partial\Omega,\ t>0 \end{aligned} \tag{1}$$

where $g = g(|\nabla G_\sigma * u|)$ is the Gaussian function, $I(x)$ is the original image, $u(x,t)$ is its smoothed version on scale t, λ is a parameter, $(u-I)$ is a term suggested by Nordstrom and $(I-g)$ is added by [31]. Since, such an anistropic diffusion (*AD*) method based on the *PDE* technique used a smoothing term, which might decrease the strength of the edges.

Recently, an efficient *AD* filter is presented in [13] by introducing a gradient magnitude operator in four directions representing more accurately the strength of the edges. This implementation of the *AD* filter is called an adaptive *AD* filter. In an adaptive *AD* filter, the selection of the parameter is done automatically. The gradient magnitude operator in Eq. (1) is sensitive to noise, especially when the strength of the edge is weak. In order to improve this situation, the following form of gradient magnitude in 4-directions was proposed [13] which can be defined as:

$$S(i,j) = \left(\frac{(\sum_{d \in W,E,S,N} |\nabla I_d(i,j)|^2)}{4} \right)^{1/2} \tag{2}$$

where d denotes the four directions (W, E, S, N), along which gradient magnitude is calculated. As pointed out before, the *AD* filter is used to remove noise. In practice, when it is applied as a preprocessing step in a melanoma *CAD* system it might diffuse the tumor's patterns.

Xie et al. [32] proposed another novel automated hair removal algorithm based on *PDE*. In this paper, the authors paid much attention to hair lines detection and then used an inpainting method based on *PDE* to remove lines. Fig. 2(b) shows the result produce by this hair-repaired algorithm. The simple non-linear diffusion filter is defined as:

$$\frac{\partial u}{\partial t} div(c(x,y,t)\nabla u) \tag{3}$$

The scalar diffusivity $c(x, y, t)$, in a pixel (x,y) at iteration or time t is chosen as a non-increasing function $g(.)$ of the gradient ∇u, which is defined by Eq. (4).

$$c(x,y,t) = g(\nabla u) = \frac{1}{(1+(\nabla u/k)^2)} \tag{4}$$

The parameter k is the gradient threshold value. Non-linear partial differential equation (*PDE*) of Eq. (3) is given by:

$$u^{t+1}(x,y) = u^t(x,y) + \lambda/n \sum_{P \in D} c(\nabla^t u(x,y))\nabla^t u(x,y) \tag{5}$$

where (x,y) is the pixel coordinates, D is the neighborhood of (x,y) pixel, n is the number of neighborhood pixels, the positive constant λ denotes smooth degree and t is the iteration time.

2.3. Hair removal by exemplar-based inpainting methods

Non-linear-*PDE* based inpainting methods are inpainting approaches that are not based on texture and, therefore, they are not suitable for hair removal in dermoscopic algorithms. Texture-based inpainting methods are used to fill missing information by texture synthesis technique and therefore are suitable for restoring the damaged region saving the structure of the image. The inpainting technique which combines non-linear-*PDE* diffusion and texture synthesis methods, is called exemplar-based inpainting. In general, the exemplar-based technique presented in [33] combines the strengths of both approaches into a single, efficient algorithm.

A few hair removal methods based on exemplar-based inpainting algorithms [12,34,35] were also proposed in the literature. In these inpainting methods a special attention is paid to linear structures. Within these structural elements, the lines abutting the target region only influence the fill order of what is at core an exemplar-based texture synthesis algorithm. The result is an algorithm that has the efficiency and qualitative performance of exemplar-based texture synthesis, which also respects the image constraints imposed by the surrounding linear structures. However, according to our knowledge [12], the number of iterations and the size of the processing window are required; parameters which are difficult to determine in general. A more detailed description of exemplar-based inpainting approaches can be found in [33]. Consequently, the exemplar-based inpainting method does not provide, in practice, an effective solution for hair removal, obtaining less impressive results than expected. Therefore, for melanoma *CAD* tool, a non-iterative and effective hair removal algorithm is needed.

3. Proposed hair removal method by fast marching scheme

In this section, we present a novel hair repaired algorithm that does not interfere with the tumor's texture. Moreover, this hair-repairing algorithm is easily combined in melanoma *CAD* tool. This approach restores the information occluded by hairs of any thickness, ruler markings and blood vessels.

The proposed hair removal algorithm is divided into three steps: (a) hair detection with the use of a derivative of Gaussian (*DOG*) [12], (b) refinement by morphological techniques and (c) then hair repair by fast marching image inpainting [36] technique. This last approach was utilized because its speed and effectiveness. The schematic of the proposed hair removal algorithm is displayed in Fig. 2. The following sections described these three steps in details.

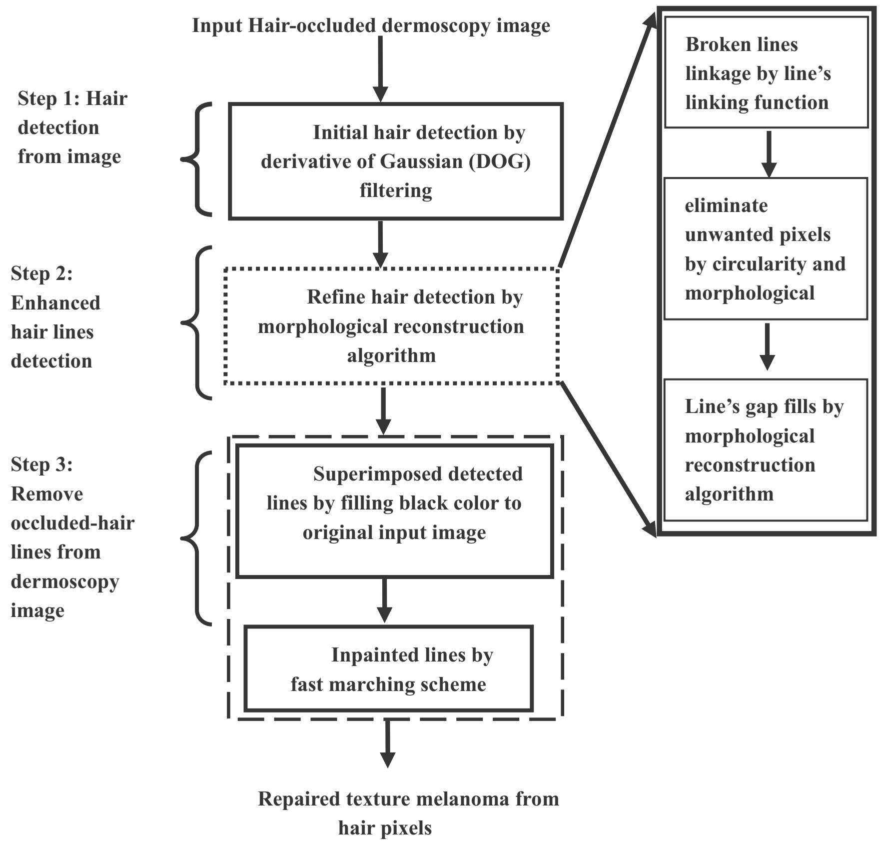

Fig. 2. Systematic flow diagram of the proposed hair-occluded information repair algorithm.

3.1. Hair detection from dermoscopy images

In the past, many hair-occluded information detection methods have been proposed. In fact, many of them detected dark hair and some detected thin hair. Moreover, many hair detection techniques assumed that hair pixels are much darker than skin or tumor area. However in practice, many dermoscopic images have hair pixels of a color that is only slightly darker than the surrounding areas. In addition to this, dermoscopic images often contain blood vessels and ruler markings.

3.1.1. Initial hair-like artifacts segmentation

To address these issues, an efficient hair detection method for hair-curvature lines, blood vessels, and ruler markings using line's detection method was developed in [12]. In the current study, we improve this method by changing the color space from *RGB* to the perceptually uniform *CIE* $L^*a^*b^*$ [37] one and extending the approach by linking the lines along with morphological methods. The concept of uniform color space refers to the fact that, in this color system, the Euclidean distances [38] among colors are related to their perceived similarity. Therefore, the use of such a color space will bring the results closer to the expected ones.

To detect accurate lines from dermoscopic images, some properties are defined to distinguish them from neighborhood pixels. These properties can be defined as thickness, magnitude, and length in addition to direction. The lesion features, on the other hand, can be distinguished because they do not have these properties. The hair line's detection scheme based on the *2-D* derivatives of a Gaussian of the luminance component (L^*) of the image in the *CIE* $L^*a^*b^*$ color space for different thickness lines is calculated as:

$$R_i(x,y) = g_i(x,y) * i(x,y) + g_\theta(x,y) * i(x,y) \tag{6}$$

where $i(x, y)$ is the L^* component of the input image, * is a convolution operator, and $g_i(x, y)$ is the Gaussian derivative for thin smooth lines calculated by Eq. (7) along with $g_\theta(x, y)$ for thick lines detection by Eq. (8). We are using *2-D* convolution (*) operator instead of multiplication because it performed smoothing function both in the *x* direction, and then in the *y* direction. The use of L^* adapts the algorithm to human perception because the luminance in this uniform color space is design to match the perceptual lightness response of the human visual system. The *2-D* derivative of Gaussian (*DOG*) for smooth thin lines detection filter is defined as:

$$g_i(x,y) = \frac{-x}{\sqrt{2\pi}.\sigma_i^3} e^{\frac{-x^2}{2\sigma_i^2}}, \quad \text{for } |x| \le 3\sigma_i, \quad |y| \le L_i/2 \tag{7}$$

This derivative of Gaussian (DOG) efficiently detects lines in all directions. Where σ_i is the standard deviation of the Gaussian function at a scale *i*, and L_i is the span of the filter in *y* direction at that scale. Parameter L_i is used to smooth a line along its tangent direction. Then the rotation of $g_i(x, y)$ with angle θ is applied using $g_i^\theta(x', y') = g_i(x, y)$, where $x' = x\cos\theta + y\sin\theta$ and $y' = y\cos\theta - x\sin\theta$. There are also some lines such as blood vessels, which are significantly thicker than normal ruler markings or hair lines. In order to achieve this characteristic, a Gaussian function with weight towards the centre of the image is defined as:

$$g_\theta(x,y) = \cos\left(\frac{\pi x'}{2\alpha}\right) \cos\left(\frac{\pi y'}{\alpha}\right) e^{-(x^2+y^2)/2(0.5\alpha)^2} \tag{8}$$

where α is the fixed parameter with a value of 0.5. The line direction is determined as the direction with maximal centreline [12] filter. The line width can be approximated by measuring the distance between a local maximum and local minimum along the perpendicular direction of the line. After the center is obtained, the direction and the width of the lines can be interpolated through the

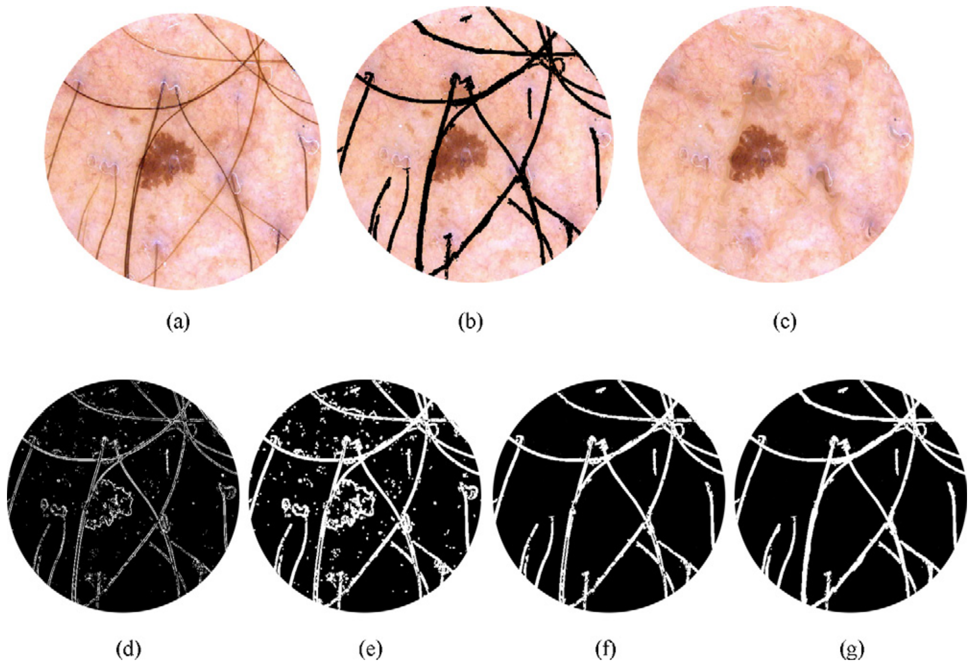

Fig. 3. A result of the proposed hair-occluded repairing method by fast marching scheme.

information calculated by a thresholding procedure. In order to calculate an automatic thresholded value, we follow the thresholded method in an iterative way, which has been developed by Ridler and Calvard in 1978. In this simple thresholding method, first the algorithm computes the mean intensity values of an image. Next, using these threshold values, it computes mean values, which are above and below to these mean intensity values. Finally, this algorithm applied iterative method to find out threshold value. By calculating these properties, unwanted curves, part of tumor structure, can be eliminated. Fig. 3(d) illustrates the hair segmentation [12] algorithm result. For detailed information of this method, the readers refer to [12].

3.1.2. Refinement of hair segmentation lines

Weak areas of hair-occluded lines may be broken by this hair detection method. In that case, line's linking function is often required. Herein, we have developed an effective line's linking function. For this reason, all detected lines are scanned in an image. Using two pixels linking function, we connected these lines, which are 10–20 pixels apart from each other in all 8-different directions. For the experimental data set, 10–20 pixels are enough to scan. It can be noticed from Fig. 3(e) that segmented hair lines are also contained contour or curvature like objects.

These contours like curves may be the part of tumor area or dermoscopic-gel. Therefore, in order to get hair lines without these contour objects, the estimated circularity and morphological area-opening conditions are imposed. For quantifying circularity, we used the method developed by Haralick [39], which is based on mean and variance of radial distances. Using this circularity condition, we have effectively segmented hair mask. Moreover, to neglect unwanted small objects such as shown in Fig. 3(e), we used the morphological area-opening function. To neglect unwanted small objects, we used 90-pixels parameter value in the morphological area-opening function along with circularity condition. The unwanted objects are filtered out if they were circular and having an area greater than 90 pixels. By removing unwanted objects from hair mask, hair segmentation result is obtained as illustrated in Fig. 3(f).

For inpainting these lines, it is necessary to smooth and fill them. Therefore to obtain smooth hair lines, morphological operators (dilation and filling) are applied to a mask image that constrains the transformation with a structuring element that defines the connectivity. In this approach the 8-pixel connectivity structuring element used in all directions. After defining this structuring element, an image dilation operation is applied on the binary mask image. As shown in Fig. 3(f), some detected lines have some gaps therefore, a morphological area-filling function is performed on the dilated mask. However, before applying area-filling operator, it is necessary to fill the holes in the image which define the outline of each line to be filled.

Let $M(x,y)$ denote a dilated binary mask image and suppose that we choose the hole filling image P, to be 0 everywhere except on the image line's border, where it is set to $(1-M(x,y))$:

$$P(x,y)=\begin{cases}1-M(x,y) & \text{if}\,(x,y)\,\text{is on the border of}\,M\\ 0 & \text{otherwise}\end{cases} \tag{9}$$

Then

$$\text{Hole\_mask}=[R_{M^c}(P)]^c \tag{10}$$

is a binary filled hair-mask image, as illustrated in Fig. 3(g). Where $R_{M^c}(P)$ denotes the reconstruction of $M(x,y)$ image from $P(x,y)$. In this way, Hole_mask(x,y) image is obtained along with x and y coordinates. The line segments extracted after the line point filling operation are shown with black color in Fig. 3(b). Next, these detected lines are inpainted by fast marching scheme as shown in Fig. 3(c).

3.2. Texture-area restoration of hair-occluded information

To repair hair-occluded information from dermoscopy images, the fast inpainting method is utilized and improved by introducing a perceptually uniform color space. Bornemann and Marz [36] developed a fast non-iterative image inpainting method in the non-uniform *RGB* color space. This lead to an algorithm not related to human perception and therefore with results that may not agree with the ones provided by a human being. In the proposed approach, this fast inpainting method is updated by transforming the image from the *RGB* color space where they were stored to the *CIE* $L^*a^*b^*$ uniform color space trying to build a human perception related algorithm.

The inpainting technique utilize a fast marching method to traverse the inpainting domain while, transporting the image values in a coherence direction by means of a structure tensor. Through the measure of the strength of the coherence, this inpainting technique switches between diffusion and directional transport. By adding this robust coherence strength, the fast marching inpainting method is more effective than other inpainting methods such as exemplar-based one. As shown in results, this method is approximately 37% more effective for region-filling than the exemplar-based inpainting technique, removing the noise without damaging the patterns and texture part of the lesion shown in Fig. 3(c). As a result, we utilized this non-iterative, fast and reliable inpainting method for removing the hair pixels from dermoscopy images. The detailed description and numerical stability of this non-iterative and effective image inpainting method can be found in [36]. However, a brief description of this repair algorithm is presented. First, a brief description of iterative *PDE* and non-iterative *PDE* is presented.

Notice that from Eqs. (1) and (5), in the diffusion step an iteration factor is always required (u^t). The simplest transport version of Eqs. (1) and (5) by neglecting some anistropic diffusion steps is defined by Bertalmio et al. [40] for image $u(x, y)$ as:

$$u^t(x, y) = \nabla^{\perp}\Delta u(x, y)\nabla\delta, \quad \delta = \Delta u(x, y) \tag{11}$$

where the measure of smoothness δ of the image is $u(x, y)$, which is transported along the field of isophotes induced by the vector field $\nabla^{\perp}\Delta u(x, y)$. Notice that from Eq. (11), the smoothing factor (δ) appears on the left side, and therefore, it is not a transport equation for δ. The simplest version of Eq. (11) can be written as:

$$u^t(x, y) = -\nabla^{\perp}\Delta u(x, y)\nabla u(x, y) \tag{12}$$

It is clear from Eq. (12) that this equation is really a transport equation for image $u(x,y)$ [41]. However, the formal stationary state of Eq. (11) defined based on edges is given as follows:

$$\vec{c}\Delta u(x, y) = 0, \quad \vec{c} = \nabla^t\Delta u(x, y) \tag{13}$$

Eq. (13) is the formal version of transported equation, which transports the image values along continues of edges from the boundary of the inpainting domain into its interior. Moreover, this transport equation strongly diffuses image area and creates 'peculiar transport patterns'. Therefore, Bornemann and Marz [36] defined a more approximate transport equation as:

$$\vec{n}\nabla u(x, y) = 0 \tag{14}$$

where $\vec{n}$ denoted the field level lines of the distance map. Eq. (14) clearly represents the advantage of this inpainting method as compared to exemplar-based method. Eq. (14) is the single-pass version of Eqs. (5) and (11). The transport direction obtained by Eq. (14) is an unsuccessful choice as suggested by Bertalmio et al. for the propagation of image information because it creates peculiar transport patterns. Therefore, a coherence direction is needed.

Image inpainting developed in [36] by fast marching scheme consists of two main concepts: (a) modifying the weighted function (b) increasing of the robustness of the method by replacing the edge-oriented transport direction of Bertalmio et al. method by the coherence direction.

To choose an appropriate weighted function $w(x,y)$ for single-pass inpainting algorithm, the authors [36] defined normalized directional dependence w as:

$$w(x, y) = (\pi/2)^{1/2}\mu/|x - y| \exp(-\mu^2/2\epsilon^2\left|\vec{c}^{\perp}(x)(x - y)\right|^2) \tag{15}$$

The advantage of this fast inpainting method over others is that it uses a directional vector $\vec{c}$ aligned with the level lines (isophotes) of image u. As shown in Eq. (12), the time variable should be stabilized and edge-directional flow should be introduced for faster and effective inpainting method. For these reasons, the integral differential equation by a hybrid splitting scheme was developed as:

$$u^t(x, y) = -\nabla^{\perp}\Delta u_{\sigma}(x, y)\nabla u(x, y) \tag{16}$$

and

$$u_{\sigma}(x, y) = k_{\sigma}u(x, y), \quad k_{\sigma}(x) = \frac{1}{2\pi\sigma^2}\exp\left(-\frac{|x|^2}{2\sigma^2}\right) \tag{17}$$

Then, formal stationary of Eq. (17) is given by:

$$\pm\nabla^{\perp}\Delta u_{\sigma}(x, y)\nabla u(x, y) = 0 \tag{18}$$

While transport equation of Eq. (18) known as edge-direction flow equation can be defined as:

$$\vec{c}(x) = \nabla^{\perp}\Delta u_{\sigma}(x, y) \tag{19}$$

Coherence direction is determined using a robust structure tensor approach followed by Weickert [42]. Therefore, the structure tensor J_p of image $u(x,y)$ is given by:

$$J_p(\nabla u_{\sigma}(x, y)) = k_p(\nabla u_{\sigma}(x, y) \otimes \nabla u_{\sigma}(x, y)) \tag{20}$$

Hence, the coherence direction

$$\vec{c}(x, y) = \vec{w}_1 \tag{21}$$

where w_1 is the normalized eigenvector to the minimal eigenvalue of $J_p(\nabla u_{\sigma}(x, y))$ on a second-moment at scale p. Moreover, the modify form of structure tensor for color images is defined in [36] for *RGB* color space ($u = (u_R, u_G, u_B)$) as follows:

$$J^m_{\sigma,p}|u = 0.299J^m_{\sigma,p}|u_R + 0.587J^m_{\sigma,p}|u_G + 0.114J^m_{\sigma,p}|u_B \tag{22}$$

Since, as it was already mentioned the *RGB* color space is not correlated to human vision. Therefore, Eq. (22) is not adapted to human perception and could lead to undesirable results like some blurring effect. To avoid this problem we choose the uniform color space *CIE* $L^*a^*b^*$, enhancing the structure tensor equation:

$$J^m_{\sigma,p}|u = 0.412453\,J^m_{\sigma,p}|u_{a^+} + 0.715160\,J^m_{\sigma,p}|u_{a^-} + 0.950227J^m_{\sigma,p}|u_b \tag{23}$$

In this manner the algorithm achieves a degree of adaptation to the human visual system that is not achieved by its original version [36]. The constant values in Eq. (23) are obtained from *RGB* to *CIE* $L^*a^*b^*$, transform matrix.

4. Experimental results analysis

4.1. Dermoscopy data set

A comparative study is performed on 100 dermoscopy images data set consisting of pigmented (65) and non-pigmented (35) skin lesions. These dermoscopic images were obtained from different sources with most of them from the department of Dermatology, Health Waikato New Zealand. In addition, most of these skin cancer images were captured from Nikon 995 with the digital acquisition system. The images have been stored in the RGB-color format with dimensions vary from 640 × 480 to 640 × 405 or 620 × 300 to 340 × 460. The dermoscopy images in this data set are of six categories consisting of: (1) 20 benign melanocytic lesions, (2) 20 malignant melanoma lesions, and (3) 25 non-melanocytic lesions, with, (4) 10 basal cell carcinoma lesions, (5) 15 Merkel cell carcinoma lesions and (6) 10 different non-pigmented lesions. Due

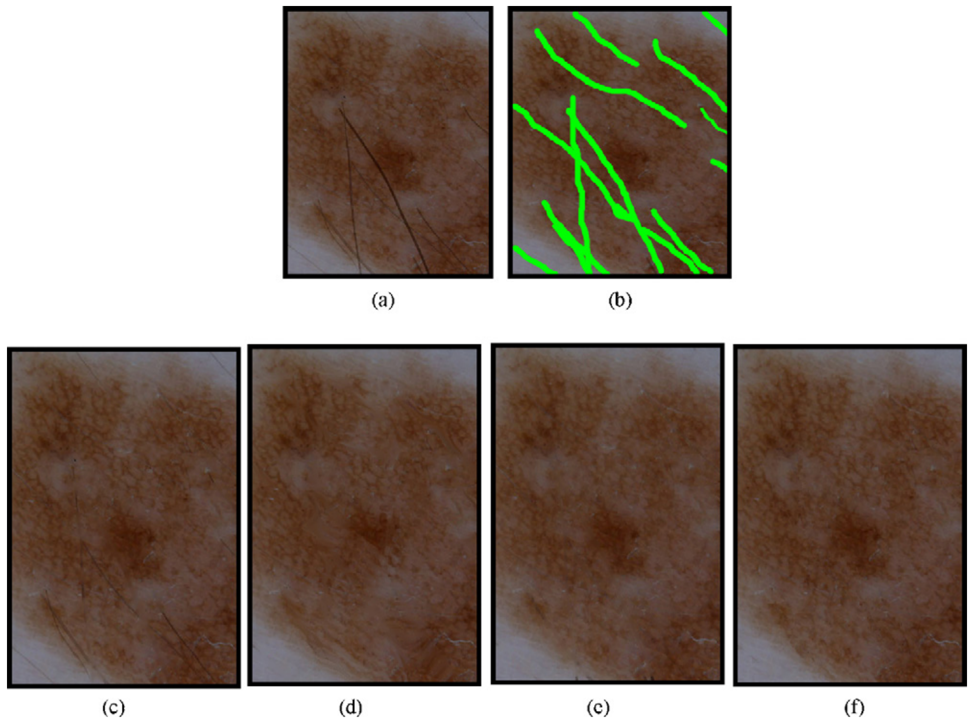

Fig. 4. Comparison results with 3 state-of-the-art hair detection methods ((c) DullRazor, (d) *PDE*-non-linear inpainting and (e) exemplar-based inpainting) along with proposed hair removal (f) algorithm.

to comparative study for hair detection procedure, we requested a dermatologist to draw the hair lines manually subsequently denoted in this paper as the hair mask. The hair mask obtained by the expert served as the "gold standard" against which the performances of various hair detection methods were compared. The data set was contained a visible hair-artifact and each image in the data set on average contains below 40% hair pixels surrounded the tumor area.

4.2. Implementation analysis tools

The software tools used were Matlab 7.6.0.324® (The Mathworks, Natick, *MA*) and C. For computational analysis, the calculations were performed on an *IBM* ThinkPad 2.0 *GHz* dual-core Intel *CPU* with 1 *GB DDR2 RAM*, running Windows 7.

4.3. Evaluation metrics

To estimate the accuracy of the proposed and the other state-of-the-art methods, we report statistical evaluation metrics. The Hammoude distance (*HM*) metric is employed to measure the hair detection error (*HDE*). *HDE* was computed by *HM* metric providing a pixel by pixel comparison. We denote (*At*) for the automatic calculated hair detection and (*GT*) for ground truth hair detection. The *GT* is measured by an expert dermatologist. *At* and *GT* vector values in each line region are calculated after measuring the number of pixels; using 4-connected component labeling algorithm. Next, the number of pixels in each hair line is counted. The hair detection error (*HDE*) metric is calculated as follows:

$$\text{Hair detection error}\,(HDE) = (\text{count}(At \cup GT) - \text{count}(At \cap GT)/\text{count}(At \cup GT)) \times 100\% \quad (24)$$

Tumor disturb pattern (*TDP*) analysis is also performed to measure the effect of hair-repaired algorithms in dermoscopy images. The intended purpose of *TDP* is to provide the statistical way to compare the different hair-repairing methods in terms of hair repairing but not detection. According to our knowledge, many hair removal algorithms were proposed but none of them calculated the effect of hair removal on tumor texture part. As mentioned before if an ineffective hair algorithm is applied before melanoma classification, then the results will not further use for classification. To overcome this problem, it is necessary to measure the effect of hair removal for each algorithm. Hence, to repair the texture of the melanoma from hair, the algorithm must be consistent with the human vision. In order to calculate *TDP*, a texture analysis scheme based on the co-occurrence matrix is utilized. The co-occurrence matrix consists of contrast (*Cn*), correlation (*Cr*), variance (*Vr*) and entropy (*Ent*) information in L^* component of *CIE* $L^*a^*b^*$, color space. First, the texture analysis by this matrix was applied on the original image (*O*) containing hair and hair-repaired (*R*) image. Next, a difference operation was performed for each information (*Cn, Cr, Vr, Ent*) of both images obtaining the COM_{or} metric. Finally, the significance texture-weighted value is also calculated by measuring the texture analysis information from image obtained by manual hair detection and repaired by developed fast marching method. In practice, texture-weighted (κ_ω) value is crucial to find out from any hair-repaired algorithms such as Dullrazor or exemplar-based methods. However, the calculated value (κ_ω) can be effectively measured from our proposed method. In order to do statistical analysis, we have fixed its minimum and maximum range from 0% to 100%. It is cleared that the hair-repaired algorithm, which returns greater value is ineffective as compared to other one. As a result, this significance value is used to measure the consequences of hair-repairing algorithms on melanoma texture part.

The difference step is calculated by Eq. (25).

$$COM_{or} = (OCn - RCn) + (OCr - RCr) + (OVr - RVr) + (OEnt - REnt) \quad (25)$$

Table 1
Comparison of hair-occluded removal algorithms performance for 100 psl and non-psl dermoscopy images in terms of mean *HDE*, *TDP* and average computational complexity.

Cited Source	Lines detection methods	Hair-repaired methods	[a]*HDE* (%)	[b]*TDP* (%)	[c]*T*(*s*)
[25]	Morphological closing operation	Bilinear interpolation	12.5	23.11	09.24
[32]	Morphological closing + thresholding	*PDE*-based inpainting	8.5	15.17	14.57
[12]	Derivative of Gaussian (DOG)	Exemplar-based inpainting	6.23	10.52	58.25
	Proposed DOG + morphological operation	Fast marching inpainting	3.21	4.48	3.80

[a] Mean hair detection error = *HDE* in percentage.
[b] Mean tumor disturb pattern = *TDP* in percentage.
[c] Average running time of line's detection and hair repaired method = *T*(*s*) in seconds.

Table 2
Comparison of proposed hair-occluded removal algorithms for color spaces in terms of mean *HDE*, *TDP* and average computational complexity.

Color spaces	Lines detection methods	Hair-repaired methods	[a]*HDE* (%)	[b]*TDP* (%)	[c]*T*(*s*)
RGB	DOG + morphological operation	Fast marching inpainting	3.21	4.48	3.80
CIELab	DOG + morphological operation	Fast marching inpainting	2.98	4.21	4.76

[a] Mean hair detection error = *HDE* in percentage.
[b] Mean tumor disturb pattern = *TDP* in percentage.
[c] Average running time of line's detection and hair repaired method = *T*(*s*) in seconds.

And the significance texture-weighted value is given by:

$$\kappa_\omega = \left(\frac{(Cn + Cr + Vr + \ Ent)}{4}\right) 100 \tag{26}$$

Finally, the *TDP* metric is derived as:

$$TDP = \left| \left(\kappa_\omega - \frac{COM_{or}}{4}\right) 100\% \right| \tag{27}$$

4.4. Comparative results and discussions

The statistical metrics *HDE* and *TDP* are computed to make the comparisons with the melanoma texture hair-repaired algorithm and the other three selected state-of-the-art methods. Linear interpolation [25], *PDE*-non-linear diffusion [32] and exemplar-based inpainting [12] are the three different hair-repairing algorithms employed in the comparative study. Moreover, the proposed algorithm related to human vision developed in the *CIE* $L^*a^*b^*$ uniform color space is also included. On 100 dermoscopic images, the numerical results of the comparative study in terms of performance and complexity are presented in Table 1. From Table 1 and Fig. 4, we see that our method gives better results than others. The detail discussions of these comparisons are explained in the subsequent subsections.

To compare our hair-repaired method with other, *RGB* non-uniform color space was used. First, our method was implemented in RGB color space. We have done this because all other [12,25,32] hair-removal methods were developed in *RGB* color space. Finally, the proposed method is implemented in *CIE* $L^*a^*b^*$ uniform color space.

4.4.1. Comparisons to linear interpolation methods

Linear interpolation [25] method like DullRazor is used to remove thin and thick dark hair. However, hair pixels with a color slightly different to the tumor color are not detected as shown in Fig. 4(c). Also as linear interpolation method uses 2 pixels neighborhood to inpaint, the detected area provide diffused patterns (see Fig. 4(c)). Therefore, for melanoma pattern extraction or recognition, DullRazor hair-repaired algorithm should not be a better choice. On mean result, image inpainted by fast marching scheme is *HDE*: 3.21%, *TDP*: 4.48% and average *T*: 3.80*s* as compared to DullRazor which is *HDE*: 12.5%, *TDP*: 23.11% and average *T*: 09.24*s*. T parameter represents the running time (in seconds) of both algorithms. As shown in Fig. 4(f), the proposed hair-repaired algorithm repairs the occluded information in a manner that is closer to human vision without disturbing the tumor's patterns. By computing the strength of the coherence, this inpainting method switches between diffusion and directional transport. Therefore, this hair removal inpainted method does not disturb the tumor's patterns. It must be noticed that the proposed hair detection and restoration algorithm posses a mean *TDP* of 4.48%. In fact, the *TDP* of the proposed algorithm is large because the original image contains hair but, in practice, this value is not high when the texture melanoma tumors are repaired and then compared with the original one.

4.4.2. Comparisons to PDE-based inpainted methods

Partial differential equations (*PDEs*) based non-linear hair removal methods have been also proposed in the past. In the beginning, Chung and Sapiro [30] developed a hair removal method by *PDE*-based diffusion equations. Recently, Xie et al. [32] proposed hair removal algorithm based on *PDE*. In this paper, the authors paid much attention to hair lines detection and then used inpainting method by *PDE* to remove lines. As discussed before, the *PDE*-based inpainted methods are time consuming techniques and what is worst; the inpaint of the detected area produces some negative effect on the patterns (see Fig. 4(e)). Therefore, for automated melanoma pattern extraction or recognition, *PDE*-based diffusion algorithm should also not be an effective solution. On mean result, image inpainted by fast marching scheme has the following values of the measured quantities *HDE*: 3.21%, *TDP*: 4.48% and average *T*: 3.80*s* while *PDE*-based diffusion [32] algorithm provides *HDE*: 8.5%, *TDP*: 15.17% and average *T*: 14.57*s*. Our method obtained effective results from *PDE* because of use of robust structure tensor, which switches between diffusion and directional transport.

4.4.3. Comparisons to exemplar-based inpainted methods

Non-linear-*PDE* based methods are not texture-based inpainting methods and, it was previously mentioned, these kinds of methods are not suitable for hair removal in dermoscopic images. In contrast to this, the inpainting technique that combines non-linear-*PDE* diffusion and texture synthesis methods, called exemplar-based inpainting method are better than linear interpolation or *PDE* based techniques as shown in Fig. 4(f). Unfortunately, these techniques require some experimental parameters to be fixed, leading in undesirable results. In addition, these computationally complex methods, in the presence of heavy hair more than 40%, cannot determine inpainted direction, which will make this method infinite. Therefore, this kind of inpainting algorithm is

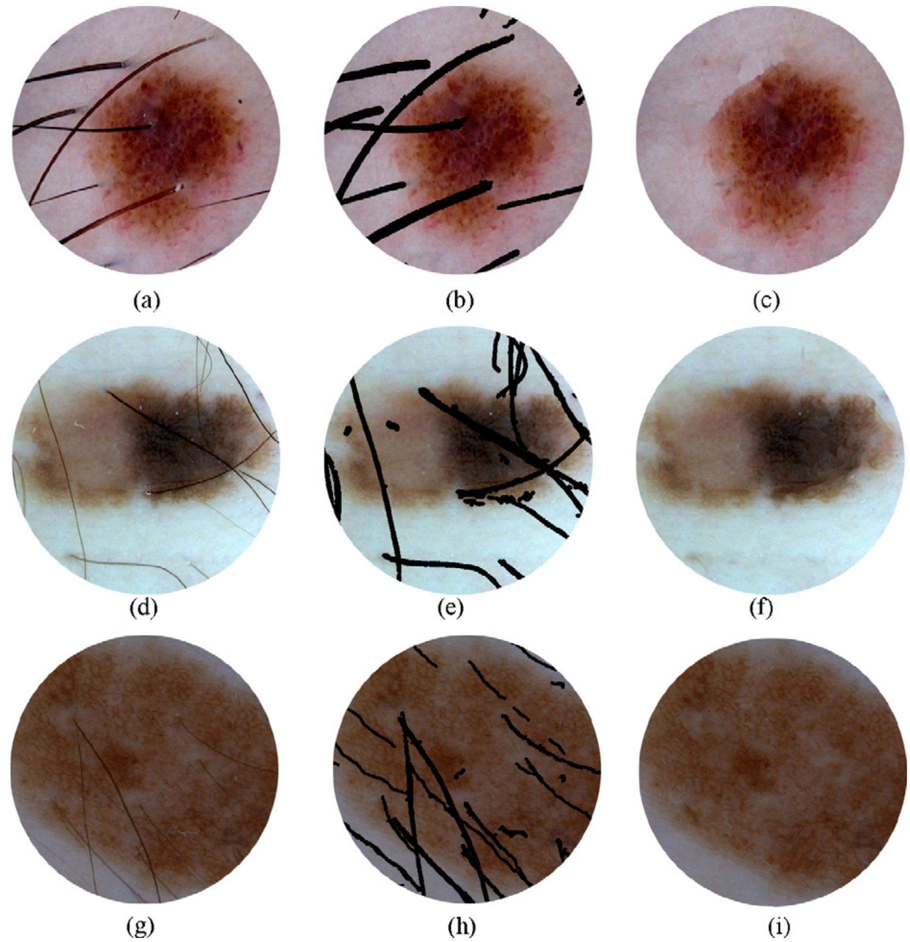

Fig. 5. Proposed hair removal algorithm by fast marching provides effective melanoma texture repairing result without damaging patterns, which shows (a, d, g) input images (b, e, h) detected lines superimposed and (c, f, i) indicate final hair removal results.

not effective on. On mean result, image inpainted by fast marching scheme is characterized by *HDE*: 3.21%, *TDP*: 4.48% and average *T*: 3.80*s* and exemplar-based method [12] is characterized by *HDE*: 6.23%, *TDP*: 10.52% and average *T*: 58.25*s*.

4.4.4. Comparisons to color spaces

Table 2 summarizes the mean *HDE* and *TDP* error along with the average running time of the proposed method in *RGB* and *CIE* $L^*a^*b^*$. This test was also performed on 100 dermoscopic images. As shown in Table 2, using uniform color space (*CIE* $L^*a^*b^*$), the hair detection and repairing algorithm is greatly enhanced. However, the running time of the proposed algorithm in terms of uniform color space is slightly more than in non-uniform RGB color space. Therefore, we adopted proposed hair-occluded information repairing algorithm in terms of uniform color space.

5. Conclusions

In this paper a comparative study of the state-of-the-art algorithms for automatic detection of hair and restoration of the texture-part of tumors from occluded information is presented, along with a novel approach based on a fast marching scheme in the *CIE* $L^*a^*b^*$ uniform color space. This comparative study is essential to reduce undesired segmentation and classification results of melanoma and other pigmented lesions, affected by the presence of the hairs covering it. In the past, many algorithms have been designed to overcome this problem, but none of them resulted in an effective and efficient technique worthy to include in any *CAD* tool for melanoma diagnosis. Moreover, many of the hair removal algorithms proposed in the literature, disturb the texture present in the lesion dramatically affecting the quality of the results.

Three hair-repairing techniques have been compared: linear interpolation, inpainting by *PDE*-based diffusion and exemplar-based. We obtained two main advantages of using the fast inpainting method as compared to other inpainting algorithms. Firstly, this method used non-iterative *PDEs*. Secondly, the main advantage of using this fast marching hair-repaired algorithm is that it utilized the structure tensor to robustly determine coherence direction that switches between diffusion and directional transport. The characteristics presented in this method are not implemented in other inpainting techniques such as exemplar-based on. For comparisons purpose in terms of performance and effectiveness, these methods have been evaluated by means of the hair detection error (*HDR*) and tumor disturbs pattern (*TDP*) analysis metric. Also, the computational complexity of each hair-repairing algorithm was computed. The manual hair segmentation of an expert dermatologist has been used as the gold standard of the comparison. The results show the low performance of the three state-of-the-art techniques when compared to the proposed one, mainly because their dependence with experimentally fixed parameters, and high complexity. The repaired pixels disturb the overall texture pattern with the consequent increase in error. However, the effectiveness of hair segmentation and repairing algorithm will be decreased in case of heavily hair pixel surrounding the tumor areas. Moreover, there are skin lesions with characteristics similar to hair pixels such as telangectasia and pigmented network tumors, which can be making difficult for hair detection procedure.

The fast hair segmentation method adapted to human perception and effective hair removal algorithm uses texture information in a way which does not disturb the tumor's pattern (see Fig. 5) when repairing the hair pixels. Hence, an accurate hair removal algorithm should be included in any automatic melanoma classification (*CAD*) system as a preprocessing step, and regarding the results, the method based on the improved fast marching scheme should be the preferred one.

Acknowledgement

This study was supported by the Chinese Scholarship Council (CSC) (grant no. 2008GXZ143).

References

[1] M.J. Sneyd, B. Cox, Melanoma in Maori, Asian and Pacific peoples in New Zealand, Cancer Epidemiol. Biomarkers Prev. 18 (2009) 1706–1713.
[2] M.E. Celebi, H. Iyatomi, G. Schaefer, W.V. Stoecker, Lesion border detection in dermoscopy Images, Comput. Med. Imag. Grap. 33 (2008) 148–153.
[3] G. Argenziano, H.P. Soyer, S. Chimenti, R. Talamini, R. Corona, F. Sera, et al., Dermoscopy of pigmented skin lesions: results of a consensus meeting via the internet, J. Am. Acad. Dermatol. 48 (2003) 679–693.
[4] H. Ganster, A. Pinz, R. Rohrer, E. Wilding, M. Binder, H. Kittler, Automated melanoma recognition, IEEE Trans. Med. Imaging 20 (2001) 223–239.
[5] R.H. Johr, Dermoscopy:, Alternative melanocytic algorithms. The ABCD rule of dermatoscopy, menzies scoring method, and 7-point checklist, Clin. Dermatol. 20 (2002) 240–247.
[6] P Rubegni, G. Cevenini, M. Burroni, R. Perotti, G.D. Eva, P. Sbano, et al., Automated diagnosis of pigmented skin lesions, Int. J. Cancer 101 (2002) 576–580.
[7] F. Ercal, M. Moganti, W.V. Stoecker, R.H. Moss, Detection of skin tumor boundaries in color Images, IEEE Trans. Med. Imaging 12 (1993) 624–627.
[8] L. Xu, M. Jackowski, A. Goshtasby, D. Roseman, S. Bines, C. Yu, et al., Segmentation of skin cancer images, Image Vision Comput. 17 (1999) 65–74.
[9] M.E. Celebi, H.A. Kingravi, B. Uddin, H. Iyatomi, Y.A. Aslandogan, W.V. Stoecker, R.H. Moss, A methodological approach to the classification of dermoscopy images, Comput. Med. Imag. Grap. 31 (2007) 362–371.
[10] K. Hoffmann, T. Gambichler, A. Rick, M. Kreutz, M. Anschuetz, T. Grunendick, et al., Diagnostic and neural analysis of skin cancer (DANAOS). A multicentre study for collection and computer-aided analysis of data from pigmented skin lesions using digital dermoscopy, Br. J. Dermatol. 149 (2003) 801–809.
[11] Q. Abbas, I.F. Garcia, M. Rashid, Automatic skin tumour border detection for digital dermoscopy using a novel digital image analysis scheme, Br. J. Biomed. Sci. 67 (2010) 177–183.
[12] Q. Abbas, I. Fondon, M. Rashid, Unsupervised skin lesions border detection via two-dimensional image analysis, Comput. Meth. Prog. Bio. (2010).
[13] J. Tang, A multi-directional GVF snake for the segmentation of skin cancer images, J. Pattern Recogn. 42 (2009) 1172–1179.
[14] B. Erkol, R.H. Moss, R.H. Stanley, et al., Automatic lesion boundary detection in dermoscopy images using gradient vector flow snakes, Skin Res. Technol. 11 (2005) 17–26.
[15] H. Iyatomi, H. Oka, M.E. Celebi, M. Hashimoto, M. Hagiwara, et al., An improved internet-based Melanoma screening system with dermatologist-like tumor area extraction algorithm, Comput. Med. Imag. Grap. 32 (2008) 566–579.
[16] J.E. Golston, R.H. Moss, W.V. Stoecker, Boundary detection in skin tumor images: an overall approach and a radial search algorithm, Pattern Recogn. 23 (1990) 1235–1247.
[17] Z. Zhang, W.V. Stoecker, R.H. Moss, Border detection on digitized skin tumor images, IEEE Trans. Med. Imaging 19 (2000) 1128–1143.
[18] H. Zhou, G. Schaefer, A. Sadka, M.E. Celebi, Anisotropic mean shift based fuzzy c-means segmentation of dermoscopy images, IEEE J. Sel. Top. Signa. 3 (2009) 26–34.
[19] D.D. GÓMEZ, C. Butakoff, B.K. Ersboll, W.V. Stoecker, Independent histogram pursuit for segmentation of skin lesions, IEEE Trans. Biomed. Eng. 55 (2008) 157–161.
[20] F. Ercal, A. Chawla, W.V. Stoecker, H.C. Lee, R.H. Moss, Neural network diagnosis of malignant melanomas from color images, IEEE Trans. Biomed. Eng. 41 (1994) 837–845.
[21] C. Grana, G. Pellacani, R. Cucchiara, S. Seidenari, A new algorithm for border description of polarized light surface microscopic images of pigmented skin lesions, IEEE Trans. Med. Imaging 22 (2003) 959–964.
[22] T. Tanaka, S. Torii, I. Kabuta, K. Shimizu, M. Tanaka, Pattern classification of nevus with texture analysis, IEEJ Trans. Electr. Electron. Eng. 3 (2008) 143–150.
[23] H. Iyatomi, H. Oka, M.E. Celebi, K. Ogawa, G. Argenziano, H.P. Soyer, H. Koga, T. Saida, et al., Computer-based classification of dermoscopy images of melanocytic lesions on acral volar skin, J. Invest. Dermatol. 128 (2008) 2049–2054.
[24] C. Serrano, B. Acha, Pattern analysis of dermoscopic images based on Markov random fields, J. Pattern Recogn. 42 (2009) 1052–1057.
[25] T.K. Lee, V. Ng, R. Gallagher, A. Coldman, D. McLean, A Dullrazor, Software approach to hair removal from images, J. Comput. Biol. Med. 27 (1997) 533–543.
[26] N.H. Nguyen, T.K. Lee, M.S. Atkinsa, Segmentation of light and dark hair in dermoscopic images: a hybrid approach using a universal kernel, Proc. SPIE Med. Imaging (2010) 1–8.
[27] P. Schmid, Segmentation of digitized dermatoscopic images by two-dimensional color clustering, IEEE Trans. Med. Imaging 18 (1999) 164–171.
[28] P.-S. Saugeona, J. Guillodb, J.-P. Thiran, Towards a computer-aided diagnosis system for pigmented skin lesions, Comput. Med. Imag. Grap. 27 (2003) 65–78.
[29] M. Fleming, C. Steger, J. Zhang, J. Gao, A. Cognetta, I. Pollak, C. Dyer, Techniques for a structural analysis of dermatoscopic imagery, Comput. Med. Imag. Grap. 22 (1998) 375–389.
[30] D.H. Chung, G. Sapiro, Segmentation skin lesions with partial-differential-equation-based image processing algorithms, IEEE Trans. Med. Imaging 19 (2000) 763–767.
[31] C.A.Z. Barcelos, V.B. Pires, An automatic based nonlinear diffusion equations scheme for skin lesion segmentation, Appl. Math. Comput. 215 (2009) 251–261.
[32] F.-Y. Xie, S.-Y. Qin, Z.-G. Jiang, R.-S. Meng, PDE-based unsupervised repair of hair-occluded information in dermoscopy images of melanoma, Comput. Med. Imag. Grap. 33 (2009) 275–282.
[33] A. Criminisi, P. Perez, K. Toyama, Region filling and object removal by exemplar-based Image inpainting, IEEE Trans. Image Process. 13 (2004) 1–13.
[34] P. Wighton, T.K. Lee, M.S. Atkinsa, Dermoscopic hair disocclusion using inpainting, in: Proc. SPIE Med. Imaging, 2008, pp. 1–8.
[35] H. Zhou, M. Chen, R. Gass, J.M. Rehg, L. Ferris, J. Ho, et al., Feature-preserving artifact removal from dermoscopy images, in: Proc. SPIE Med. Imaging, 2008, pp. 1–9.
[36] F. Bornemann, T. März, Fast image inpainting based on coherence transport, J. Math. Imaging Vis. 28 (2007) 259–278.
[37] V. Vezhnevets, V. Sazonov, A. Andreeva, A survey on pixel-based skin color detection techniques, Proc GraphiCon. (2003) 85–92.
[38] M.J. Garrett, M.D. Fairchild, A top down description of S-CIELAB and CIEDE2000, Color Res. Appl. 28 (2003) 425–435.
[39] R.M. Haralick, A measure for circularity of digital figures, IEEE Trans Syst. Man Cybern. SMC-4 (1974) 394–396.
[40] M. Bertalmio, G. Sapiro, V. Caselles, C. Ballester, Image inpainting, Proc. Sig Graph. Conf. Comput. Graph. Interactive Tech. (2000) 417–424.
[41] M. Bertalmio, G. Sapiro, V. Caselles, C. Ballester, Navier–Stokes, fluid dynamics, and image and video inpainting, in: Proc. CVPR IEEE Int. Conf. Computer Vision and Pattern Recognition, 2001, pp. 355–362.
[42] J. Weickert, Coherence-enhancing shock filters, Lecture Notes Comput. Sci. 2781 (2003) 1–8.